

CAVITY QUENCH STUDIES IN Nb₃Sn USING TEMPERATURE MAPPING AND SURFACE ANALYSIS OF CAVITY CUT-OUTS*

D.L. Hall[†], M. Liepe, R.D. Porter, P. Cueva, D.B. Liarte, D.A. Muller, J.P. Sethna
Cornell Laboratory for Accelerator-Based Sciences and Education (CLASSE),
Ithaca, NY 14853, USA

Abstract

Previous experimental studies on single-cell Nb₃Sn cavities have shown that the cause of quench is isolated to a localised defect on the cavity surface. Here, cavity temperature mapping has been used to investigate cavity quench behaviour in an Nb₃Sn cavity by measuring the temperature at the quench location as the RF field approaches the quench field. The heating profile observed at the quench location prior to quench appears to suggest quantised vortex entry at a defect. To investigate further, the quench region has been removed from the cavity and analysed using SEM methods. These results are compared to theoretical models describing two vortex entry defect candidates: regions of thin-layer tin-depleted Nb₃Sn on the cavity surface that lower the flux entry field, and grain boundaries acting as Josephson junctions with a lower critical current than the surrounding material. A theoretical model of layer growth developed using density functional theory is used to discuss alterations to the coating process that could mitigate the formation of such defects.

INTRODUCTION

Single-cell 1.3 GHz ILC-style niobium cavities coated with Nb₃Sn have outperformed the efficiency of their niobium equivalents while operating at 4.2 K and 16 MV/m [1–3]. However, all Nb₃Sn cavities coated at Cornell are limited to quench fields between 14 and 18 MV/m. Pulsed testing [4] has demonstrated that higher fields can be achieved, but fall still short of the theoretical maximum field that Nb₃Sn could achieve given its superheating field of approximately 400 mT.

To better understand this limitation in quench field, temperature mapping studies were performed on a single-cell 1.3 GHz Nb₃Sn cavity to observe the behaviour of the cavity near the quench field. Following data taking, the cavity was cut to remove the origin the quench region, as well as representative samples from other regions of the cavity.

EXPERIMENTAL METHOD

The temperature mapping system in use at Cornell University is an array of cryogenic temperature sensors that are mounted onto a single-cell 1.3 GHz cavity, as seen in Fig. 1. Composed of 646 sensors, each one a 100 Ω (at room temperature) carbon resistor, the array is mounted on 38 boards equipped with 17 sensors each that surround the cavity. Through the use of set screws, the resistors are

pressed against the cavity surface, with good thermal contact being ensured through the application of thermal paste to each sensor head. Each sensor is capable of a resolution of 1 mK or less at a bath temperature of 2.0 K.

The temperature map can be operated in one of three modes. In the most basic mode, the cavity is kept at a constant RF power while the voltage across each sensor (equivalent to its temperature via a known calibration) is measured. Such a measurement takes approximately 15 minutes per acquisition. In the second mode, the cavity is allowed to quench multiple times while the system scans board-per-board, searching for sudden spikes in temperature associated with a cavity quench. In this mode, the resolution of the system is sorely impacted, but due to the large temperature spikes associated with a quench, this is not a problem for the purposes of the measurement. This particular mode results in a *quench map*, indicating the location(s) of the cavity quench.

A third mode was designed specifically for this experiment, dubbed *single-scan* mode, in which a single sensor is scanned at high speed – 20 kHz – while maintaining the high resolution of the temperature mapping basic mode. The sacrifice to be made is that only a single sensor can be operational at any one time. However, for the purposes of monitoring a specific location, such as the region known to be the centre of the cavity quench, this mode is ideal.

For this study of the quench dynamics, one of the best-performing Cornell Nb₃Sn cavities was chosen: a single-

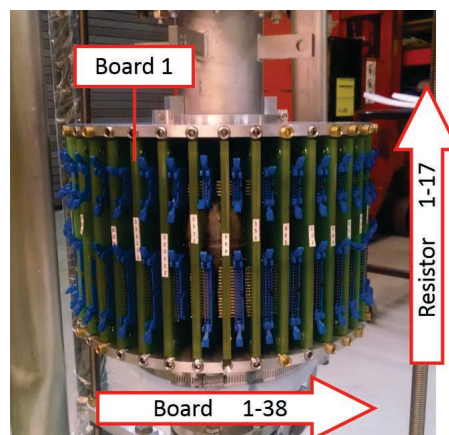


Figure 1: The single-cell temperature mapping system in use at Cornell University, mounted onto a 1.3 GHz single-cell ILC-style cavity coated with Nb₃Sn. The cables connecting the boards to the data acquisition system have been removed for better visibility.

* This work was primarily supported by U.S. DOE award DE-SC0008431.

[†] dlh269@cornell.edu

Content from this work may be used under the terms of the CC BY 3.0 licence (© 2017). Any distribution of this work must maintain attribution to the author(s), title of the work, publisher, and DOI.

cell, 1.3 GHz, ILC-style cavity dubbed LTE1-7, which has shown Q 's of greater than 10^{10} at 4.2 K and 16 MV/m [2]. The cavity received the current standard Cornell coating, consisting of a 5 hour nucleation step, 1.5 hours of coating with the cavity at 1120°C and the source at 1250°C, followed by a 1 hour annealing step with the source and cavity at 1120°C [2]. The cavity can sustain fields up to 17-18 MV/m before being limited by quench.

TEMPERATURE MAPPING RESULTS

An example of a single-scan trace is shown in Fig. 2. A trigger signal initiates the acquisition of the chosen sensor on the temperature map, as well as the power meter monitoring the transmitted power from the cavity. From a previously obtained calibration factor, this transmitted power measurement provides a measurement of the peak RF field in the cavity. Shortly after the trigger signal is sent, the RF power is turned on, and the power in the cavity is allowed to raise to a maximum level determined by the Q_0 of the cavity and the power setting on the amplifier. Provided the cavity does not quench, the RF power will be turned off approximately 20 seconds afterwards, whereupon the cavity is allowed to ring down. After 50 seconds, the acquisition is complete.

The quench field of an Nb₃Sn cavity, once known, is precisely defined and highly repeatable. This allows operation at only 2-4 mT beneath the quench field of the cavity. By carefully increasing the power setting on the amplifier, the field at which the cavity equilibrates can be set to be just beneath the quench field. After the quench location was established using quench mapping, the cavity was cycled above the critical temperature to release the flux trapped during the quench mapping, recovering the high quality factor of the cavity. The sensors near the origin of the quench location were then analysed using the single-scan method.

As the equilibrated field in the cavity was brought closer to the quench field (although never actually allowing the

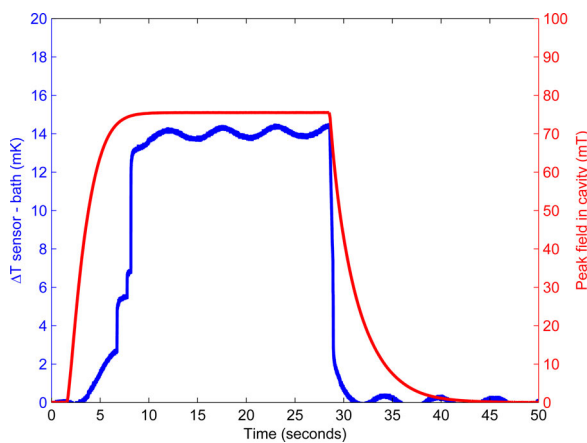


Figure 2: A single-scan trace, showing the RF field in the cavity (in red) and the temperature of the sensor at located at the quench origin (in blue). The oscillations seen on the temperature signal are due to the valve oscillations from the pumping system that keeps the bath temperature at 2.0 K.

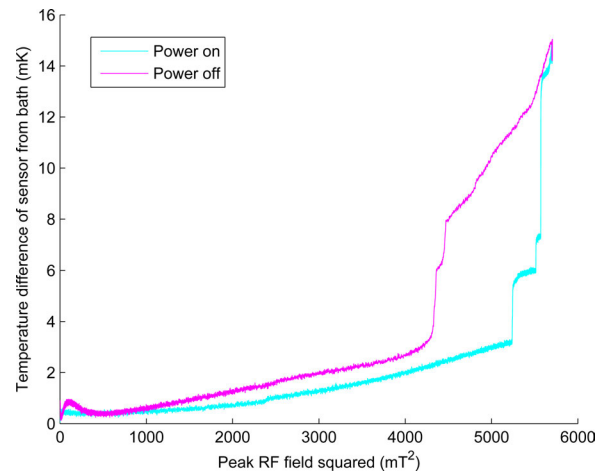


Figure 3: A plot of the ΔT of the sensor at the quench origin with respect to the bath versus the square of the RF magnetic field in the cavity. In this plot, Ohmic losses appear as a linear dependence. The cyan line is data obtained as the cavity powered up, while the magenta line was obtained as the cavity was allowed to ring down.

cavity to quench, as this would cause the Q_0 to degrade significantly and require a thermal cycling), sudden jumps in temperature were seen on the sensor immediately on top of the quench location. These jumps were found to be highly repeatable, always happening at the same level of RF field in the cavity, and always showing the same jump in temperature across multiple scans.

By plotting the square of the peak RF field in the cavity as a function of the temperature difference of the sensor from the helium bath, as shown in Fig. 3, the phenomenon is evident. When plotted against B^2 , ohmic losses appear as a linear dependence in ΔT . The jumps in temperature are evident at higher fields, as is the significant hysteresis seen between when the cavity powers up vs. when it rings down.

CAVITY CUT-OUTS

After analysis using the temperature mapping system, the cavity was removed from the insert and the region surrounding the origin of the quench was removed. This was done on a CNC milling machine, with particular care being taken to remove metal chips as they generated by the cutting bit. Air cooling was used to ensure that the part did not exceed 35-50°C, and low cutting and table feed speeds were used to minimise the amount of vibration experienced by the part. At the end of cutting, no traces of cracks or metal shards could be found beyond approximately 1-2 mm of the cut edge.

After the quench origin was removed, three more samples were cut: one from the equator region and one from either half-cell of the cavity, for comparison to the quench region. Again, care was applied to minimise damage or contamination of the sample coupon. Chemical analysis using EDS revealed no major differences in stoichiometry and chemical composition between the four different regions of the cavity, reaffirming that over a scale of square millimetres the cav-

Content from this work may be used under the terms of the CC BY 3.0 licence (© 2017). Any distribution of this work must maintain attribution to the author(s), title of the work, publisher, and DOI.

ity coating is uniform across the entire cell. Therefore, any defect that will lead to cavity quench must be small, on the order of 1-10 μm .

CANDIDATES FOR CAVITY QUENCH

The sudden jumps in temperature seen in Fig. 3, have – to within measurement error – a height that is an integer multiple of the smallest observed jump. This suggests quantised vortex entry, as opposed to thermal runaway at a defect. The particular shape of the trace is very similar to that expected from vortex entry at grain boundaries acting as Josephson junctions [5]. This similarity, both in the jumps and the hysteresis, can be seen in Fig. 4, which is reproduced from Ref. [5].

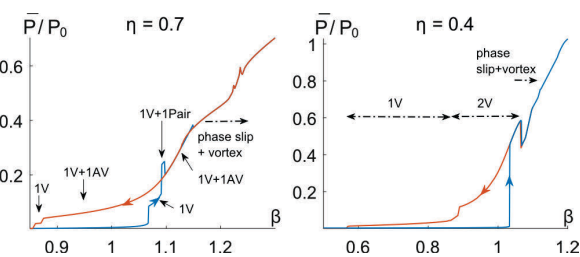


Figure 4: AC power dissipation in a grain boundary modelled as a Josephson junction, reproduced from Ref. [5]. The horizontal axis is the normalised current, β , which is proportional to the applied magnetic field. The value $\eta = 1/RC$, where R and C are the normal conducting resistance and capacitance of the junction. For values of $\eta < 1$, the losses demonstrate jumps due to vortex entry, similar in fashion to Fig. 3.

Flux entry could also occur at regions where the T_c of the material is suppressed [6], which in turn suppresses the ultimate flux entry field of the material. Such a suppression in T_c can occur due to tin-depletion of the Nb_3Sn , as off-stoichiometric phases have a lower T_c [7]. A tin-depletion of only 3% could lead to a reduction of the ultimate field down to approximately 100 mT. Grains with a tin-depletion of 1-2% have been seen in cross-sections of samples [6]; however, whether such a feature would allow for the limited, quantised flux entry suggested by Fig. 3 rather than causing an outright quench is as yet uncertain.

SEM images of the centre of the quench region, taken with a Tescan Mira3, reveal sharp features that could lead to significant field enhancement. Figure 5 demonstrates the most notable such feature found within the area of the origin of the quench. The left-most images, coloured in green, were taken with a backscatter detector operating in composition mode, thus being sensitive to changes in atomic number or large changes in surface normal vector. On the right, coloured in purple, is the same region taken with a secondary electron detector at an angle to the sample. Images taken with this detector have a higher spatial resolution, but also greater topographical contrast as well as edge glow, and so render the feature seen in the backscatter detector harder to see. However, it is clear from the wide area image and the

zoomed-in region that the feature involves a sharp change in the orientation of the surface normal, almost as if there were a crease in the material. This feature may have formed due to motion of the niobium substrate underneath – at coating temperatures, the fine grain niobium grains will grow to sizes on the order of a few millimetres, and as this growth is occurring at approximately the same that the Nb_3Sn layer is growing the interaction of the two layers may have formed this feature. The sharpness of this feature suggests that it may cause significant field enhancement, and so be a prime candidate for a quench origin. However, it does not reveal the exact mechanism that initiated the quench.

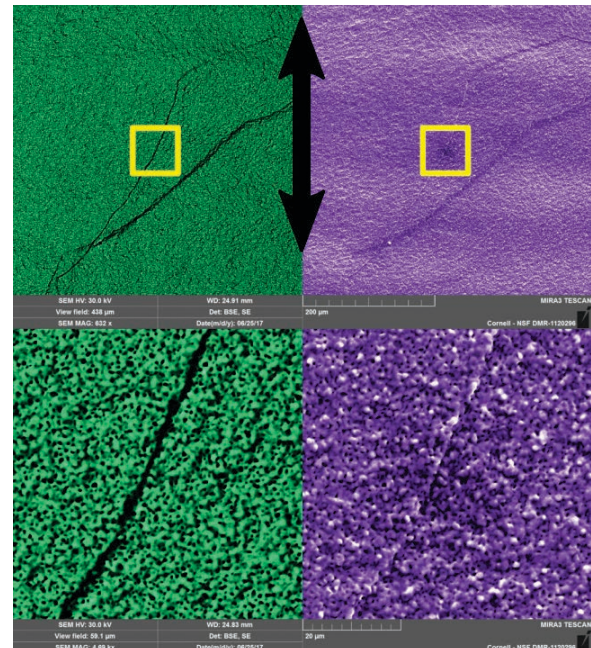


Figure 5: Scanning electron microscope images taken on a Tescan Mira3 FEG SEM. These images were taken at the quench origin as determined by the temperature map, an area roughly 6 mm by 6 mm on the cut-out. The black arrow indicates the direction of the RF magnetic field. The images have been coloured for visibility. The upper row of images is taken at a low magnification level; the lower row are images taken from the area indicated by the yellow box in the upper row. The left images were taken with a backscatter detector in composition mode; the right images were taken with a chamber (at an angle to the sample) secondary electron detector.

CONCLUSION

A quench at 18 MV/m seen in a Nb_3Sn cavity has been localised to a defect, which has been analysed using temperature mapping and subsequently removed by cutting on a milling machine. Coupons from other parts of the cavity confirm that there are no detectable large-scale changes in layer stoichiometry across the surface of the cavity.

Temperature mapping of the quench origin reveals the presence of sudden jumps in temperature as the field in

the cavity approaches the quench field, in a manner that is seemingly consistent with magnetic flux entry at a grain boundary. However, the possibility that early flux entry may be happening at tin-depleted surface grains is still being actively considered.

Scanning electron microscopy of the quench region cut-out reveals what appear to be sharp features, seemingly originating from the niobium substrate. It is possible these are being created during the grain growth of the substrate that is occurring at the coating temperatures during which the film is growing. The sharp nature of these features will lead to significant field enhancement, rendering them a prime candidate for the quench origin, if not necessarily the cause.

REFERENCES

- [1] S. Posen and D. L. Hall, “Nb₃Sn superconducting radiofrequency cavities: fabrication, results, properties, and prospects,” *Superconductor Science and Technology*, vol. 30, no. 3, p. 33004, 2017. [Online]. Available: <http://stacks.iop.org/0953-2048/30/i=3/a=033004>
- [2] D. L. Hall, M. Liepe, and J. Maniscalco, “RF Measurements on High Performance Nb₃Sn Cavities,” in *Proceedings of IPAC 2016*, Busan, May 2016. [Online]. Available: <https://doi.org/10.18429/JACoW-IPAC2016-WEPMR024>, 2016.
- [3] D. L. Hall, J. J. Kaufman, M. Liepe, R. D. Porter, and J. Sears, “First Results From New Single-Cell Nb₃Sn Cavities Coated at Cornell University,” in *Proceedings of IPAC 2017*, Copenhagen, Denmark, [Online]. Available: <https://doi.org/10.18429/JACoW-IPAC2017-M00CA2>, 2017.
- [4] S. Posen, N. Valles, and M. Liepe, “Radio Frequency Magnetic Field Limits of Nb and Nb_3Sn ,” *Phys. Rev. Lett.*, vol. 115, no. 4, p. 47001, Jul. 2015. [Online]. Available: <https://link.aps.org/doi/10.1103/PhysRevLett.115.047001>
- [5] A. Sheikzadeh and A. Gurveich, “Dynamic transition of vortices into phase slips and generation of vortex-antivortex pairs in thin film Josephson junctions under dc and ac currents,” *Physics Review B*, vol. 95, 2017.
- [6] D. L. Hall, P. Cueva, D. B. Liarte, M. Liepe, J. Maniscalco, D. A. Muller, R. D. Porter, and J. P. Sethna, “Quench Studies in Single-Cell Nb₃Sn Cavities Coated Using Vapour Diffusion,” in *Proceedings of IPAC 2017*, Copenhagen, Denmark, [Online]. Available: <https://doi.org/10.18429/JACoW-IPAC2017-MOPVA116>, 2017.
- [7] A. Godeke, “A review of the properties of Nb₃Sn and their variation with A15 composition, morphology and strain state,” *Superconductor Science and Technology*, vol. 19, no. 8, pp. R68—R80, Aug. 2006. [Online]. Available: <http://stacks.iop.org/0953-2048/19/i=8/a=R02?key=crossref.b011eb22ef1c1d3f8f2c161fc5a2d175>